Neurotherapeutics 21 (2024) e00384

Contents lists available at ScienceDirect

Neurotherapeutics

journal homepage: www.sciencedirect.com/journal/neurotherapeutics

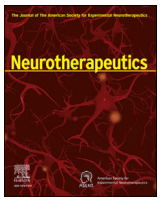

Original Article

Potentiation of the muscarinic acetylcholine receptor 1 modulates neurophysiological features in a mouse model of Rett syndrome

Hong-Wei Dong [a,b], Kelly Weiss [c,d], Kathryn Baugh [a], Mac J. Meadows [c,d], Colleen M. Niswender [b,c,d,e,f,1,*], Jeffrey L. Neul [a,b,c,f,1,*]

[a] Department of Pediatrics, Division of Neurology, Vanderbilt University Medical Center, USA
[b] Vanderbilt University Kennedy Center, Vanderbilt University Medical Center, Nashville, TN, USA
[c] Department of Pharmacology, School of Medicine, Vanderbilt University, Nashville, TN, USA
[d] Warren Center for Neuroscience Drug Discovery, School of Medicine, Vanderbilt University, Nashville, TN, USA
[e] Vanderbilt Institute for Chemical Biology, Nashville, TN, USA
[f] Vanderbilt Brain Institute, Nashville, TN, USA

ARTICLE INFO

Keywords:
Rett syndrome
Neurophysiological biomarkers
Auditory event related potential
M_1 acetylcholine receptor
Positive allosteric modulator
Mouse models

ABSTRACT

Rett syndrome (RTT) is a neurodevelopmental disorder primarily caused by mutations in the X chromosome-linked gene *Methyl-CpG Binding Protein 2* (*MECP2*). Restoring MeCP2 expression after disease onset in a mouse model of RTT reverses phenotypes, providing hope for development of treatments for RTT. Translatable biomarkers of improvement and treatment responses have the potential to accelerate both preclinical and clinical evaluation of targeted therapies in RTT. Studies in people with and mouse models of RTT have identified neurophysiological features, such as auditory event-related potentials, that correlate with disease severity, suggesting that they could be useful as biomarkers of disease improvement or early treatment response. We recently demonstrated that treatment of RTT mice with a positive allosteric modulator (PAM) of muscarinic acetylcholine subtype 1 receptor (M_1) improved phenotypes, suggesting that modulation of M_1 activity is a potential therapy in RTT. To evaluate whether neurophysiological features could be useful biomarkers to assess the effects of M_1 PAM treatment, we acutely administered the M_1 PAM VU0486846 (VU846) at doses of 1, 3, 10 and 30 mg/kg in wildtype and RTT mice. This resulted in an inverted U-shaped dose response with maximal improvement of AEP features at 3 mg/kg but with no marked effect on basal EEG power or epileptiform discharges in RTT mice and no significant changes in wildtype mice. These findings suggest that M_1 potentiation can improve neural circuit synchrony to auditory stimuli in RTT mice and that neurophysiological features have potential as pharmacodynamic or treatment-responsive biomarkers for preclinical and clinical evaluation of putative therapies in RTT.

Introduction

Rett syndrome (RTT) is a neurodevelopmental disorder (NDD) that predominantly affects girls and women and is characterized by loss of hand skills and spoken language, repetitive hand movements, and gait problems [1]. The majority of people with RTT have loss-of function mutations in the X-linked gene *Methyl-CpG-binding Protein 2* (*MECP2*), which encodes the transcriptional regulatory protein MeCP2 [2,3]. Affected individuals also exhibit a number of other clinical features such as seizures, growth failure, breathing irregularities and other autonomic abnormalities [4–7] and are dependent on caregivers for all activities of daily living throughout their lives [8].

Mouse models of RTT display numerous phenotypic abnormalities similar to clinical features found in people with RTT [1,9–11]. Restoration of *MECP2* expression in RTT mice, even after symptom onset, reverses phenotypes and provides hope for the development of meaningful disease modifying/reversing therapies in RTT [12,13]. These findings have led to the evaluation of a number of novel therapeutic approaches in RTT disease models, including modulation of glutamate signaling [14–17], treatment with growth factors [18–21], gene therapy [22–26],

* Corresponding authors.
E-mail addresses: Colleen.Niswender@Vanderbilt.edu (C.M. Niswender), jeffrey.l.neul@vumc.org (J.L. Neul).
[1] Equal contribution.

https://doi.org/10.1016/j.neurot.2024.e00384
Received 17 April 2024; Received in revised form 7 June 2024; Accepted 9 June 2024

and re-expression of MeCP2 [27–31]. A number of human clinical trials in RTT have been conducted, initiated, or proposed [15,20,32–34] including a recent successful phase 3 clinical trial and FDA approval of trofinetide, the first drug for RTT [35].

Rapid therapeutic development in RTT is hindered by the lack of well-validated biomarkers of early treatment response and clinical improvement. Biomarkers that are consistent between pre-clinical disease models and affected individuals have the potential to improve preclinical therapy evaluation, informing and accelerating efficient clinical trials. Recent work in people with RTT has detected changes in neurophysiological measures, such as changes in quantitative EEG frequency power and alterations in evoked potentials, that correlate with disease severity [36,37]. Interestingly, similar neurophysiological features have been found to correlate with phenotypic abnormalities in RTT mouse models [13,38–40], and can be normalized in mice expressing a partial loss-of-function (LOF) allele of MeCP2 by increasing expression of the partial LOF MeCP2 variant [40], suggesting that these neurophysiological features may serve as translatable biomarkers of disease progression and improvement.

Here, we characterized changes in neurophysiological features in a RTT mouse model after acute treatment with a positive allosteric modulator (PAM) targeting muscarinic acetylcholine receptor activity (mAChRs). Alterations in the expression of various mAChRs have been seen in human RTT brain autopsy samples and in animal models with RTT syndrome [41–45]. Selective removal of MeCP2 function from cholinergic neurons in mice causes phenotypic and physiological abnormalities that are similar to those seen in RTT mouse models lacking MeCP2 protein expression [46–48]. Treatment with compounds that increase cholinergic tone or selective restoration of MeCP2 function in cholinergic neurons improves phenotypes in RTT model animals [46–50]. Further, mRNA levels of the M_1, M_2, M_3 and M_5 mAChR subtypes were significantly decreased in cortical autopsy samples from people with RTT relative to unaffected cortical samples; however, only M_1 expression demonstrated a linear relationship with MeCP2 expression [44,45]. Additionally, similar decreases in M_1 expression were also found in *Mecp2*$^{+/-}$ mice, and treatment of these animals with an M_1 positive allosteric modulator (PAM), VU0453595, corrected deficits in social preference, spatial memory, associative memory deficits, and apneas [45]. In the present study, we evaluated changes to neurophysiological features after acute administration of an M_1 PAM, VU0486846 (VU846), to *Mecp2*$^{+/-}$ mice; we have shown this compound to be a highly selective ligand for M_1 receptors that exhibits robust pro-cognitive efficacy in animal models without cholinergic adverse effects and has a pharmacokinetic profile suitable for chronic dosing [51,52]. In the current study, we show that acute treatment with VU846 across a dose range from 1 to 30 mg/kg results in an inverted U-shaped dose-response relationship with the most robust improvement in auditory event-related potential (ERP) (also known as auditory evoked potential [AEP]) features at 3 mg/kg. These results point to the potential for translatable neurophysiological features such as AEP to be useful in preclinical as well as early-stage clinical studies to conduct dose-finding experiments and validate treatment options.

Methods

Animals

Heterozygous female *Mecp2*$^{+/-}$ (MUT) and littermate wildtype (WT) animals at 8 weeks were purchased from Jackson Laboratory (3860 B6.129P2(C)-Mecp2<tm1.1Bird>/J). All procedures used in this study adhered to the published guidelines of the National Institutes of Health and were approved by the Institutional Animal Care and Use Committee at Vanderbilt University Medical Center. Mice were maintained in an AAALAC accredited facility in 12 h light/dark cycles with food and water ad libitum.

EEG headmount implantation

Headmount implantation for EEG recording was performed at 16 weeks of age as described previously [38]. Briefly, animals were anesthetized and secured in a stereotaxic apparatus. A midline sagittal incision was made along the scalp to expose the skull. An EEG/EMG headmount (#8201-SS, Pinnacle Technology Inc.) was positioned along the middle of the exposed skull with the front edge 2.0 mm anterior to bregma, and fixed with four screw electrodes (#8209, Pinnacle Technology Inc.) at the four attachment sites of the headmount. Two stainless wires mounted to the tail of the headmount were inserted into the two side trapezius muscles for EMG recording, and the electrodes and base of the headmount were covered in fast-setting dental cement. After recovery from anesthesia and resuming free mobility, animals were returned to the vivarium and housed individually.

Compound administration

VU0486846 (VU846), a positive allosteric modulator (PAM) of the M_1 muscarinic acetylcholine receptor, was synthesized at Warren Center for Neuroscience Drug Discovery (WCNDD) of Vanderbilt University. The compound was dissolved in 10% Tween 80 and sonicated for 1 h before administration. Vehicle (10% Tween 80) and VU846 (1, 3, 10 and 30 mg/kg) were administered to *Mecp2*$^{+/-}$ and wildtype female mice via intraperitoneal (i.p.) injection. VU846 dosing started 2 weeks after headmount implantation. All the doses were administered in a randomized, within-subject design, in which animal received a dose with a week washout interval [51]. Animals were dosed from weeks 18–23 and euthanized at 24 weeks of age.

Data collection

After a two-week recovery from surgery, EEG recordings were collected from freely moving mice with EEG headmount rigidly connecting to a preamplifier system (#8202-SL, Pinnacle Technology Inc., Lawrence, KS). The signals were pre-amplified 100 × with initial high pass filter of 0.5 Hz, sampled at 400 Hz and digitized using a 14bit A/D converter and routed to a PC-based acquisition and analysis software package via USB. All EEG data were obtained using Sirenia Software from Pinnacle Technologies, Inc. Animal activity was monitored using an online camera and data were stored for offline analysis. AEPs were evoked during EEG recordings. Auditory stimuli consisted of a series of 200 white-noise pips (10-ms duration, 0.25 Hz frequency) and were generated using RVPDX software and RZ6 hardware (Tucker Davis Technologies FL) and presented through multi-field magnetic speakers (Tucker Davis Technologies, FL) which were located at a distance of 12 inches directly above the cage. Sound delivery was synchronized with EEG recordings using a TTL pulse to annotate the onset of each sound in a train. Stimuli were calibrated using a sound pressure meter at 80 ±3 dB SPL. During data collection, 1 h baseline EEG and basal AEP were recorded before either vehicle or VU846 administration. AEPs were tested again 30 min after compound administration, and 1 h EEG was subsequently recorded.

Data analysis

EEG power spectrum

The saved EEG data was first determined as Wake (continuous movement) and Sleep (prolonged periods of no movement) according to the captured video, EEG and EMG waveform [38]. Two minutes of EEG data in the Wake and Sleep states from baseline and after drug/vehicle administration were retrieved and imported into MATLAB (MathWorks, Inc) for power spectrum analysis. Spectral plots were generated with the Fast Fourier Transformation (FFT) function with rectangular binning of 1s with 50% window overlap and a spectral resolution of 0.5 Hz. The average power (μV^2/Hz) was calculated from 1 to 100 Hz and further binned into standard frequency bands: Delta (0.5–4 Hz), Theta (4–8 Hz), Alpha (8–12 Hz), Beta (12–30 Hz), low Gamma (30–55 Hz) and high Gamma (65–100

Hz). For comparisons across the individuals, the spectral power was normalized by the total power under 0–100 Hz. To investigate the potential role of abnormal neural network activities in RTT mice, and the effect of neural noise in shaping the power spectrum seen in these mice, the 1/f slope of the power spectrum was calculated in the 2–20 Hz frequency range via linear regression in log-log scale [38,53].

Auditory evoked potential (AEP)

For AEP analysis, EEG data were imported into Matlab and extracted as −100 ms to 500 ms epochs relative to the auditory stimulation. All trials were visualized in the Matlab browser. Signals from −100 ms to 0 before the stimulation were taken as the baseline. The trials shown as artificial noise, unstable baseline or epileptiform discharging were eliminated from the calculation; the grand average of AEP was then calculated for individual mice. Peak components were extracted from grand average waveforms as follows: P1 (positive deflection between 10 and 70 ms), N1 (negative deflection between 50 and 150 ms), P2 (positive deflection between 100 and 350 ms) and N2 (negative deflection between 150 ms and 400 ms) The rising-slope of the P2 phase was calculated by Δ (change) in peak amplitude (P2–N1)/Δ in peak time (P2–N1) and the decay slope of P2 was calculated by Δ peak amplitude (N2–P2)/Δ peak time (N2–P2).

Event-related spectral perturbation and inter-trial phase coherence calculations

Event-related spectral perturbation (ERSP) measures average dynamic changes in amplitude of the broad band EEG frequency spectrum as a function of time relative to the auditory stimulation. In this study, ERSP was calculated from the Morlet wavelet-transformed data according to the common methods by Cohen (Cohen 2014). The raw power values (from 0 to 500 ms) were corrected by dividing each time point by the mean activity in a pre-stimulus baseline period (−100 to 0 ms) at each frequency [54]. The resulting values were then converted to decibels (dB) by taking the base 10 logarithm.

Inter-trial phase coherence (ITPC, also referred as phase locking factor [PLF]) is a descriptive statistical measure characterizing the circular variance of even-related phase information (the phase consistency across trials). It is defined by the magnitude of the vector average of the oscillatory phases at every point of the time-frequency channel domain across the trials. A value of 0 represents random phase distribution, whereas a value of 1 represents identical phase values in all trials. In this study, ITPC was calculated from the Morlet wavelet-transformed epoch time-frequency with wavelet cycles of 6 using Matlab script derived from Cohen's method [54].

Epileptiform discharge

One hour baseline EEG and 1 h EEG post AEP detection after drug administration were exported to Clampfit 10 and bandpass filtered at 0.5–20 Hz. Waveforms were characterized as epileptiform by their spike-wave appearance with peak voltage of at least 1.5-fold of background, occurring in a rhythmic train with frequency between 6 and 10 Hz and duration of at least 0.25 s. The detected events were verified by visual

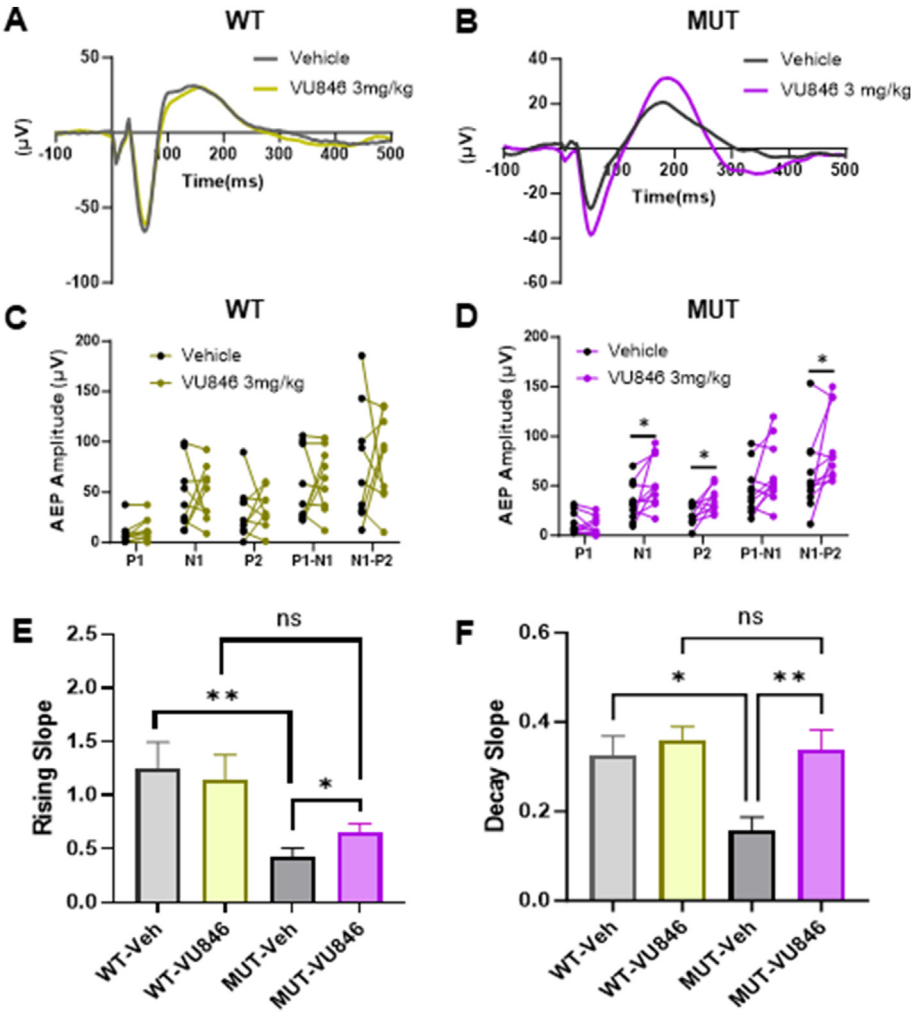

Fig. 1. Acute treatment with the M_1 PAM VU846 at 3 mg/kg improved AEP in RTT mice. A. Grand average AEP in wildtype (WT, n = 11) animals 30 min after acute injection of vehicle (gray) or 3 mg/kg VU846 (yellow), showing no change in AEP after VU846 injection. B. Grand average AEP in *Mecp2*$^{+/-}$ mice (n = 11) after vehicle (black) or 3 mg/kg VU846 (purple) injection, showing increased N1 and P2 amplitudes. C. Individual WT animal AEP peak amplitudes after vehicle or VU846 injection. D. Individual MUT animal peak amplitudes after vehicle or VU846 injection. 3 mg/kg VU846 treatment increased N1, P2 and N1–P2 amplitudes in MUT mice (*p < 0.05, paired *t*-test). E. P2 rising slope in WT and MUT animals after vehicle or 3 mg/kg VU846 injection. P2 rising slope was reduced in MUT animals compared to WT after vehicle injection but increased after VU846 injection. F. P2 decay slope in WT and MUT animals after vehicle or 3 mg/kg VU846 injection. P2 decay slope was decreased in vehicle treated MUT animals but increased to WT levels after VU846 injection. (E and F, *p < 0.05 and **p < 0.01 one-way ANOVA followed by posthoc Tukey's multiple comparisons test). (For interpretation of the references to color in this figure legend, the reader is referred to the Web version of this article).

confirmation. Incorrect detections were eliminated from the final calculation.

Statistics

Statistics and graphical representation of data were performed using Prism 9.0 (San Diego, CA). Data were expressed as mean ± SEM. Comparisons between vehicle and a specific VU846 dose within genotype were compared using paired Student's t-test. One-way ANOVA followed by posthoc Tukey multiple comparison was used when comparing the difference among multiple dosing treatments within genotype. Comparisons between genotypes under the same dose were evaluated using Student's t-test, and among the multiple doses using two-way ANOVA following by Tukey multiple comparison test. $p < 0.05$ was set as a significant difference. Statistical group comparisons of ERSP and ITPC were conducted by binning time into 240 parts and frequency into 100 parts, resulting in a 100X240 matrix. Nonparametric cluster analysis was used to determine contiguous regions in the matrix that were significantly different from a distribution of 1000 randomized Monte Carlo permutations based on previously published method [55,56]. If the cluster sizes of the real assignments (both positive and negative direction, resulting in a two-tailed alpha of $p = 0.025$) were larger than 97.25% of the random group assignments, those clusters were considered significantly different between treatment. The statistical method was described in detail in each applicable section.

Results

To assess the effect of acute M_1 PAM administration on neurophysiological features, vehicle and VU846 (1, 3, 10 and 30 mg/kg) were administered in a randomized manner to *Mecp2*$^{+/-}$ (MUT) and wildtype (WT) littermate female mice. This dose range of VU846 was chosen based on previous work which demonstrated that 10 mg/kg VU846 treatment reversed risperidone-induced deficits in contextual fear conditioning, with a minimal effective dose of 1 mg/kg and a moderate effect at 3 mg/kg [51]. We observed significant effects on various AEP parameters with the 3 mg/kg dose of VU846; to demonstrate VU846's effect on each neurophysiological feature, the data for this dose are presented first. We then used the same analysis to evaluate the drug's dose-response.

Acute injection of 3 mg/kg M_1 PAM VU846 improved auditory evoked potential peak amplitudes and waveforms in RTT mice

VU846 at 3 mg/kg and an equal volume of vehicle were administered to 11 female MUT and 11 WT mice, and AEP was evaluated before and 30 min after treatment. As previously observed in a different female RTT mouse model [38], vehicle-treated MUT animals showed alterations in AEP features compared to vehicle-treated WT animals, including decreased AEP N1 amplitude, P2 amplitude, increased P2 latency (Fig. 1A–B, Supplemental Table 1) and broadening of the P2 waveform as shown by decreased rising slope (Fig. 1E–Supplemental Table 1) and

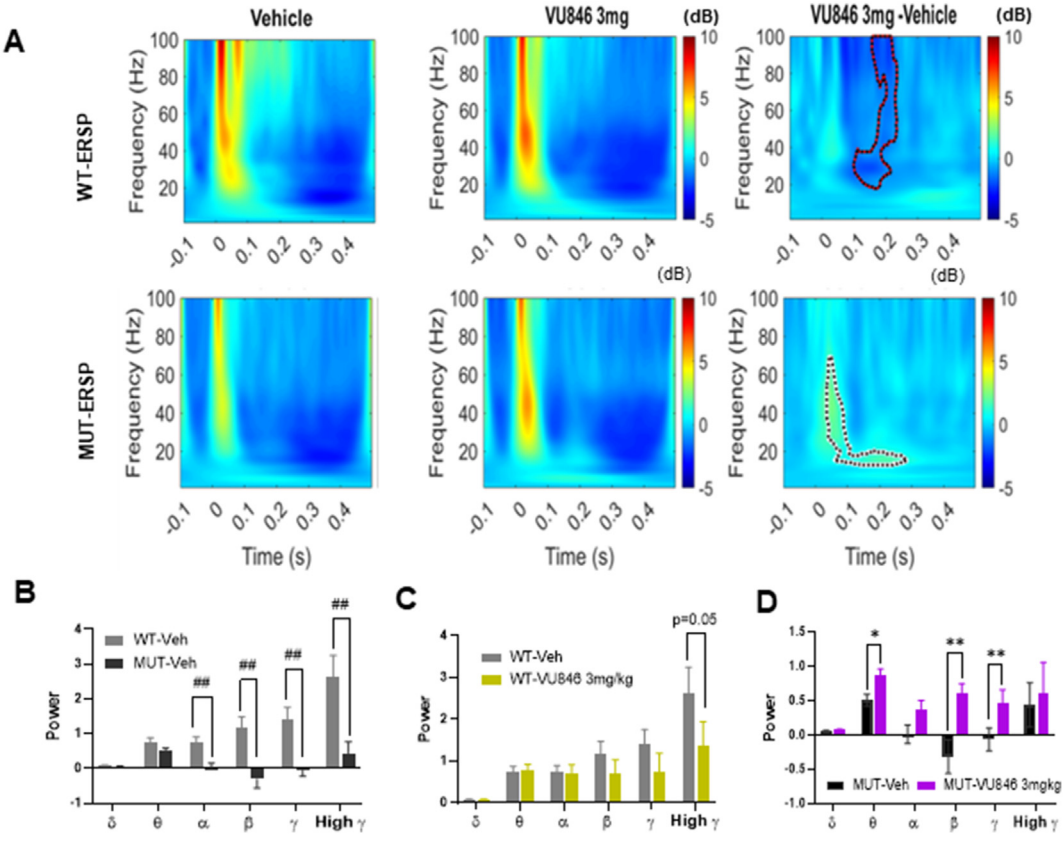

Fig. 2. Acute treatment with M_1 PAM VU846 at 3 mg/kg increased auditory ESRP in RTT mice. A. Heat maps of ESRP after auditory stimulus (time 0, X-axis) with color gradient indicating power changes (legend). WT animals are shown in the top panels and MUT animals in the bottom panels, with vehicle treatment in the left panels, VU846 treatment in the middle panels, and the difference between treatment in the right panels. The right panel shows the difference of the power (VU846-Vehicle) between treatments, with significant differences (permutation testing) outlined in the red-dotted area for WT (top right) and black-dotted area for MUT (bottom right). B. Mean ESRP in defined frequency from 0 to 250 ms after vehicle injection in WT and MUT mice (##$p < 0.01$, *t*-test comparing between genotypes). Mean frequency band ESRP in WT (C) or MUT (D) animals after vehicle or VU846 injection (*$p < 0.05$, **$p < 0.01$, paired-t-test between vehicle and VU846 injection within genotype). (For interpretation of the references to color in this figure legend, the reader is referred to the Web version of this article).

decaying slope (Fig. 1F–Supplemental Table 1). Vehicle-treated MUT animals also showed increased variability in the shape of the AEP waveform compared to vehicle-treated WT animals as demonstrated by an increased coefficient of variation (CV) of the P1 peak amplitude, P1 and N1 peak latency, and P2 rising slope (Supplemental Fig. 1A and B).

Acute treatment with VU846 (3 mg/kg, i.p.) in WT animals did not change AEP peak amplitudes (Fig. 1A–C), latency (Supplemental Table 1), P2 rising and decay slope (Fig. 1E–F) or CV of AEP features including peak, latency and P2 rising and decay slopes (Supplemental Fig. 1). In contrast, acute injection of VU846 (3 mg/kg) in MUT animals increased the N1 and P2 peak amplitudes compared to vehicle-treated control (Fig. 1 B, D); additionally, treatment increased both the N1–P2 rising slope (Fig. 1E), P2–N2 decay slope (Fig. 1F), and decreased both N1 and P2 latency CV (Supplemental Fig. 1). 3 mg/kg VU846 treatment in MUT mice did not affect AEP peak latencies (Supplemental Table 1).

Acute injection of 3 mg/kg M1 PAM VU846 improved auditory event-related power in RTT mice

Previous work using time-frequency decomposition analysis found alterations in auditory time-locked oscillatory activity in RTT mice, with changes in both auditory event-related spectral pertubation (ERSP), a measure of frequency power averaged across trials, and inter-trial phase coherence (ITPC), which assesses oscillatory phase locking across trials [39,57,58]. Because ERSP and ITPC both correlate with phenotypic severity and age in RTT mice [38,39], we sought to evaluate the effect of VU846 on these putative neurophysiological biomarkers. Consistent with prior studies, vehicle-treated MUT animals exhibited decreased auditory ERSP compared to WT animals (Fig. 2A, left panels), with decreased alpha, beta, gamma, and high gamma frequency power (Fig. 2B). Compared to vehicle injection, acute administration of 3 mg/kg VU846 in MUT animals increased high frequency (30–70Hz) ESRP in the first 100 ms after stimulation as well as low frequency (10–20Hz) ESRP between ~100 and 250 ms after stimulation (Fig. 2A, bottom right panel, black dotted area $p < 0.05$ using permutation testing). In contrast, acute injection of 3 mg/kg VU846 in WT animals did not change ESRP in the early time window (<100 ms) but decreased ESRP in frequencies >20Hz in the 100–250 ms time period after stimulation (Fig. 2B, top right panel, red dotted area $p < 0.05$ using permutation testing). We calculated ESRP power averaged over 0–250 ms for individual frequency bands and found that acute injection of 3 mg/kg VU846 in WT animals decreased high gamma ESRP but did not affect other frequency bands (Fig. 2C). Acute injection of 3 mg/kg VU846 in MUT animals increased averaged ESRP in the theta, beta, and gamma frequency bands (Fig. 2D).

Consistent with our previous findings [38], vehicle-treated MUT animals showed decreased phase locked power (ITPC) compared to vehicle-treated WT animals (Fig. 3A–B), specifically in the theta, alpha, and gamma frequency bands (Fig. 3C). Acute injection of 3 mg/kg VU846 did not change ITPC in WT animals (Fig. 3A–B, 3D), but increased ITPC in MUT animals (Fig. 3A, lower row, black dotted area), specifically in the low frequency range of 2–6 Hz (Fig. 3B, $p < 0.05$, lower row, black dotted area, permutation testing). ITPC average power between 0 and 250 ms after stimulation showed increased ITPC in delta and theta frequencies between MUT animals treated with vehicle versus VU846 (Fig. 3E). The increased phase-locked low frequency power in MUT animals after VU846 injection supports the concept that M_1 activation increases auditory stimulus-induced cortical neuronal synchrony in MUT animals, consistent with the effects on grand average AEP observed in MUT animals after VU846 injection, specifically the increased P2 amplitude

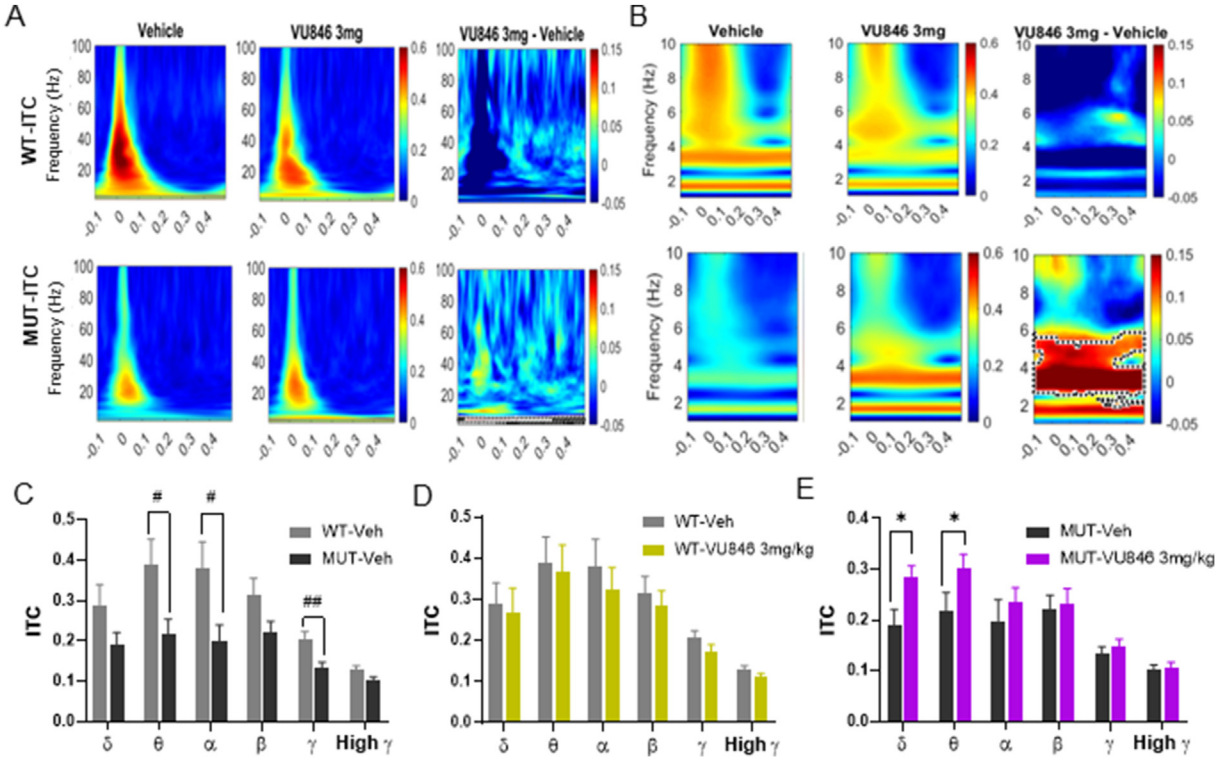

Fig. 3. Acute treatment with the M_1 PAM VU846 at 3 mg/kg increased ITPC in RTT mice. A. Heat maps showing average ITPC in WT (top row) and MUT mice (bottom row) after vehicle injection (left panels), VU846 injection (middle panels), and difference in ITPC between treatment (right panels, significant differences outlined in black-dotted area, permutation testing). B. Heat maps as in A, with frequency range displayed (y-axis) restricted to the 0–10Hz range to highlight low frequency ITPC changes observed in MUT animals after VU846 injection. C. Mean ITPC (0–250 ms) in defined frequency bands in WT and MUT animals after vehicle injection (#$p < 0.05$ and ##$p < 0.01$, *t*-test comparing between genotypes). Mean frequency band ITPC in WT (D) and MUT (E) after vehicle or VU846 injection (*$p < 0.05$, paired-t-test between vehicle and VU846 injection within genotype).

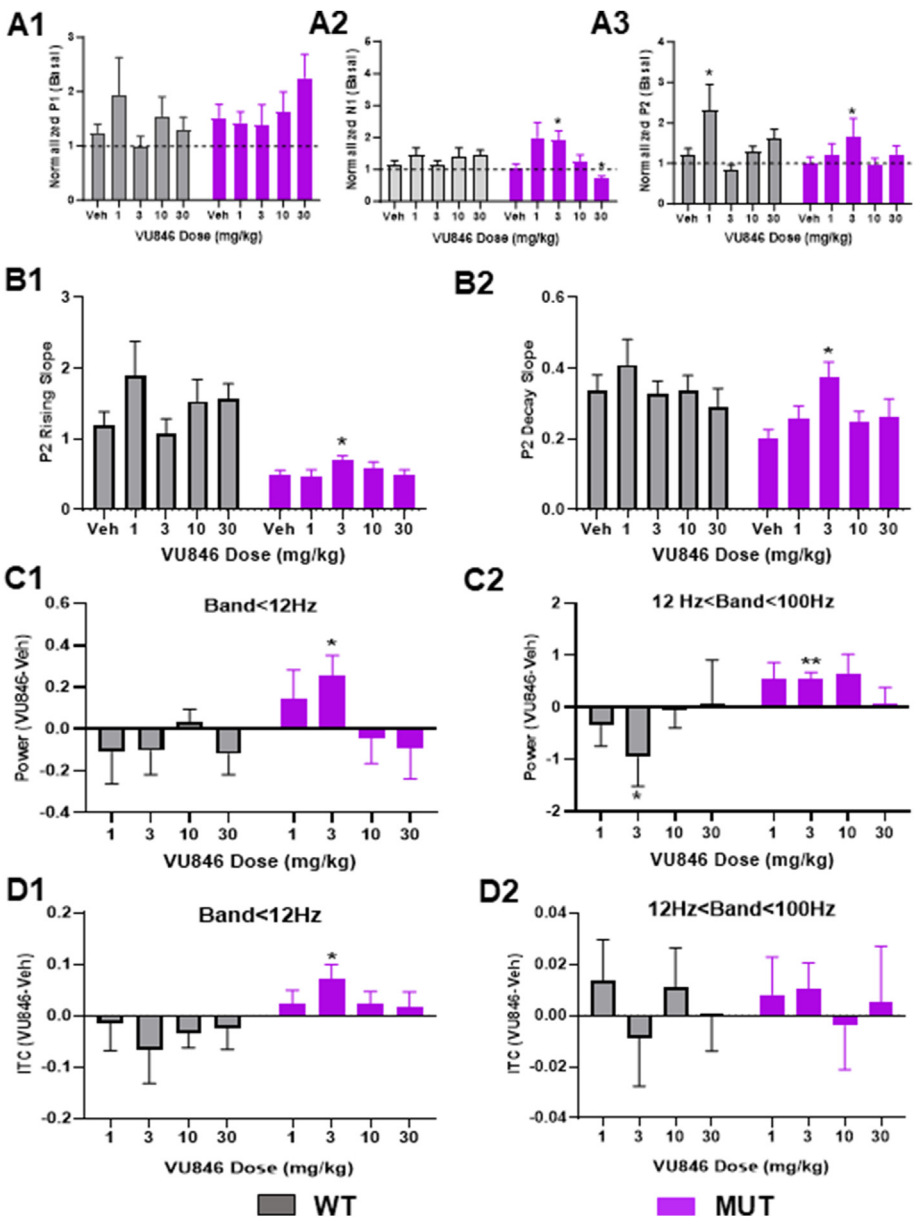

Fig. 4. Dose-response of VU846 auditory-event related features. A. Normalized AEP peak amplitudes (normalized to individual animal baseline values prior to injection: A1-P1; A2-N1; A3-P2) after treatment with vehicle or doses of VU846 indicated along the X-axis. B. VU846 dose-response effects on P2 rising (B1) and decay (B2) slopes. C. Change in ESRP after VU846 injection at various doses compared to vehicle injection in low frequency bands (C1, 0–12 Hz) and high frequency bands (C2, 12–100Hz). D. Change in ITPC after VU846 injection at various doses compared to vehicle injection in low frequency bands (C1, 0–12 Hz) and high frequency bands (C2, 12–100Hz). *p < 0.05, **p < 0.01, within genotype ANOVA with post-hoc Tukey pairwise comparison between VU846 dose and vehicle.

(Fig. 1D), increased P2 rising and decay slope (Fig. 1E–F) and decreased intra-and inter-animal AEP response variability (Supplemental Fig. 1).

Dose-dependent effect of the M1 PAM VU846 on AEP

As acute treatment of MUT animals with 3 mg/kg VU846 improved a variety of auditory-event related neurophysiological features, we evaluated the dose-dependent effects of VU846 by acutely treating WT (n = 8–13) and MUT (n = 10–14) mice with an additional range of VU846 doses (1, 10, and 30 mg/kg). To compare across doses, AEP features after vehicle or VU846 treatment were normalized to individual animal values captured immediately before treatment (Fig. 4A–B). VU846 treatment at any dose did not affect AEP latencies in WT or MUT mice (Supplemental Table 1). In WT animals, VU846 treatment only showed an effect on P2 amplitude at 1 mg/kg compared to vehicle injection, with no effect at any dose on normalized P1 amplitude, N1 amplitude, or P2 rising or decay slope (Fig. 4A–B, Supplemental Table 1). In MUT mice, 3 mg/kg injection of VU846 increased normalized N1 and P2 peak amplitudes (Fig. 4A), but this effect was not seen at other doses of VU846; however, 30 mg/kg injection of VU846 decreased the normalized N1 peak amplitude (Fig. 4A2, Supplemental Table 1). Similarly, the increase in P2 rising (Fig. 4B1) and decay slope (Fig. 4B2) was only seen after 3 mg/kg injection of VU846 and not after treatment with other VU846 doses (Supplemental Table 1). We observed a similar inverted U-shaped VU846 dose-response curve in MUT animals in the ESRP (Fig. 4C) and ITCP (Fig. 4D), with increased ESRP in low frequency bands (<12Hz, Fig. 4C1) and high frequency bands (12–100Hz, Fig. 4C2) and increased ITPC in low frequency bands (<12Hz, Fig. 4D1) only observed after injection of 3 mg/kg VU846. Aside from a decreased high frequency ESRP in WT mice after injection of 3 mg/kg VU846 (Fig. 4C2), no other changes in ESRP or ITPC were seen in WT animals at any VU846 dose (Fig. 4C–D). Overall, the inverted U-shaped dose response seen in MUT animals suggests a narrow response range for VU846.

VU846 treatment did not alter basal EEG power or epileptiform discharges

We previously found changes in basal EEG power in a mouse model of RTT with increased delta power, decreased alpha and gamma power, and increased 1/f slope between 2 and 20 Hz in MUT animals compared to WT, similar to that observed in people with RTT [36,38,53]. Here, we

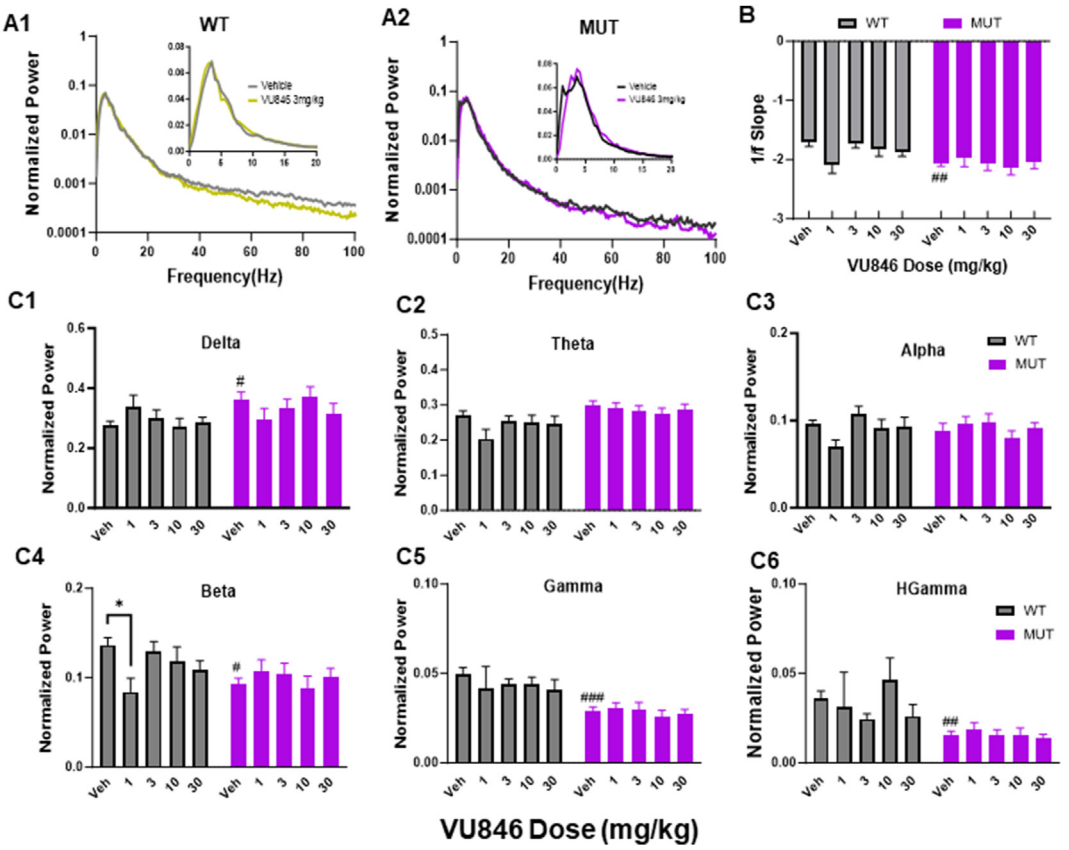

Fig. 5. EEG power spectrum after acute VU846 treatment. A. Normalized EEG power (log scaled, normalized by total power) from parietal cortex during sleep after vehicle or VU846 administration (3 mg/kg) in WT (A1) or MUT mice (A2). Insets show normalized power between 2 and 20 Hz in non-log scale. B. 1/f slope for WT and MUT animals after acute VU846 doses. C. Mean total parietal sleep EEG power in WT or MUT animals after acute dosing as indicated along the X-axis showing (C1) delta, (C2) theta, (C3) alpha, (C4) beta, (C5) gamma, and (C6) high gamma frequency band power. #p < 0.05, #p < 0.01, ###p < 0.001 between genotype comparisons after vehicle injection. *p < 0.05 within genotype comparison between VU846 and vehicle injection. Two-way ANOVA followed by Tukey's post-hoc pairwise comparison.

observed similar changes in a different RTT mouse model (Fig. 5A, parietal cortex EEG power during sleep), with increased 1/f slope (Fig. 5B), increased delta power (Fig. 5C1), and decreased beta (Fig. 5C4), gamma (Fig. 5C5), and high gamma (Fig. 5C6) in vehicle-treated MUT animals compared to vehicle-treated WT. Treatment of WT animals with 1 mg/kg VU846 decreased beta power compared to vehicle (Fig. 5C4), but did not affect other features of basal EEG at any VU846 dose (Fig. 5). VU846 treatment in MUT animals did not change EEG power or 1/f slope at any dose (Fig. 5, Supplemental Table 2). Similar results were observed in active state parietal EEG as well as frontal cortex EEG in sleep and active states (Supplemental Table 2).

As seizures and frequent epileptiform discharges are common in people with RTT [4], and frequent spontaneous epileptiform discharges have been observed in both hemizygous male and heterozygous female *Mecp2* mutant mice [38,59], we evaluated the effect of acute treatment of VU846 on epileptiform discharges in MUT mice (Fig. 6). No changes in the incidence (Fig. 6B) or duration (Fig. 6C) of epileptiform discharges was observed in any of the doses of VU846 tested.

Discussion

Recent studies in people with RTT and animal models of RTT have demonstrated consistent changes of neurophysiological features that correlate with age and clinical/phenotypic severity, suggesting the potential for these neurophysiological measures to serve as biomarkers of clinical progression [36–39,60–64]. However, it has not been determined if these neurophysiological features have the potential to serve as treatment-responsive biomarkers. In this study, we found that VU846, a PAM targeting the M_1 mAChR, improved neurophysiological features by increasing AEP peak amplitudes, enhancing auditory evoked power, and increasing stimulus-driven neuronal synchronous activity as seen by improvement of the AEP waveform and increased inter-trial phase coherence. By evaluating the dose-dependent response, we found that VU846 treatment showed an inverted dose-response effect on these AEP features with a narrow effective dose range. Additionally, VU846 treatment across a range of doses had no marked effect on basal EEG power or the frequency of epileptiform discharges. These results suggest that neurophysiological features such as AEP could serve as biomarkers to evaluate early treatment response and pharmacodynamic dose finding in preclinical trials.

The inverted U-shaped response of M_1 PAM VU846 on AEP in RTT mice suggests a narrow dose range for efficacy in this outcome measure. We previously reported the activity of a 10 mg/kg dose of another M_1 PAM, VU0453595, which effectively rescued social preference, spatial memory, and associative memory deficits in RTT mice [45]; however, dose-response experiments were not performed. Our studies here were based on the development of VU846 as an improved M_1 PAM with enhanced potency and pharmacokinetics compared to VU0453595 [51,65] as well as studies showing that acute administration of VU846 dose-dependently enhanced recognition memory in naive rats and reversed risperidone-induced deficits in acquisition of contextual fear conditioning with minimum effective dose of 3 mg/kg with no inverted U response observed [51]. Based on these findings, there appears to be a disconnect between behavioral efficacy and changes in AEP that will require cross validation of multiple M_1 PAMs in dose-response format in both behavior and EEG/AEP evaluation in RTT mice. Interestingly,

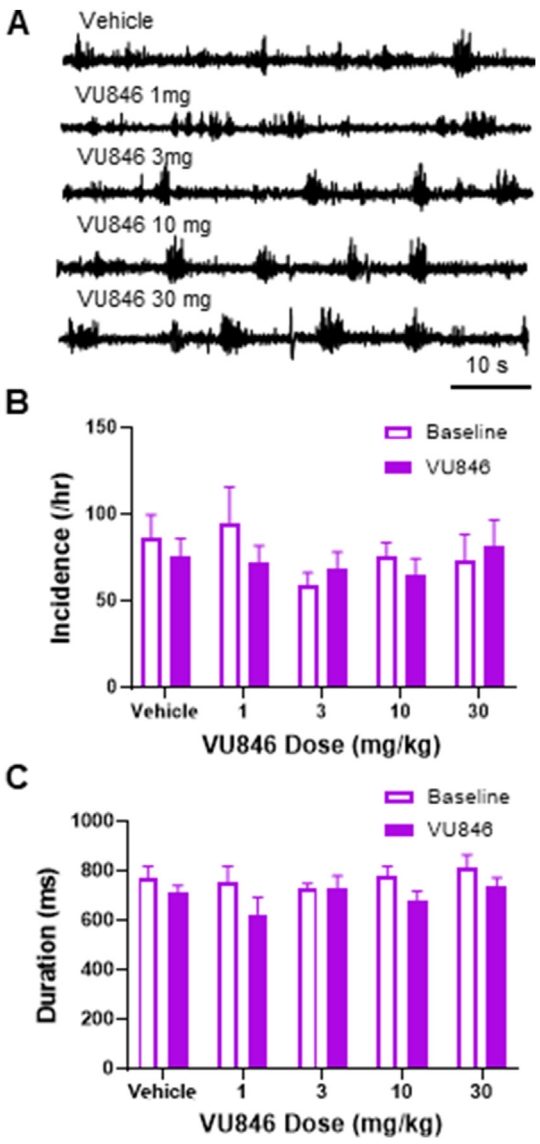

Fig. 6. VU846 has no effect on epileptiform discharges in RTT mice. A. Representative EEG traces showing epileptiform discharges in MUT mice after vehicle or VU846 injection. B. Quantitation of frequency of epileptiform discharges in MUT mice after vehicle or VU846 injection. C. Quantification of average epileptiform discharge duration after vehicle or VU846 injection.

chronic dosing of 10 mg/kg VU846 in either an Alzheimer's or a prion disease model for several weeks resulted in efficacy in reversing cognitive deficits as well as benefits in neuronal survival and amyloid processing with no loss of efficacy over time [52,66,67]. This suggests that chronic dosing of VU846 may induce differential efficacy compared to acute administration; as VU846 has been optimized for use in chronic dosing paradigms, these could form the basis of future studies. We would note, however, that a similar inverted U-shaped dose response in RTT mice was reported in our study of the of M_4 PAM VU0467154 (VU154), which rescued anxiety, social preference, associative memory, and respiratory phenotypes in RTT mice after several weeks of dosing, but benefit was seen only with 3 mg/kg but not with 1 or 10 mg/kg doses [44,68]. Based on our findings, future studies evaluating compound behavior on both behavior and AEPs with RTT mice using dose-response and chronic dosing studies would be informative in positioning AEPs as a biomarker for muscarinic mechanisms. Regardless, the studies here show that effects on AEPs are detected in RTT mice, suggesting that they have the potential to serve as translatable biomarkers for dose-finding and treatment outcomes in the clinic.

In general, the effects of PAMs are often subtle based on their mechanism of action. However, it is not unexpected to observe a more robust effect in a disease model with reduced expression of the receptors being targeted by the PAM, as seen here with the RTT mouse model. Experiments of VU846 in slices from WT mice examining the prefrontal cortex (PFC) layer V or the ventral hippocampal-PFC synapse in the prefrontal cortex from WT mice showed that the compound did not induce LTD when applied alone; however, it potentiated the LTD induced by mAChR agonists [51]. In contrast, in vivo treatment of naïve WT rats with VU846 showed a dose-dependent improvement in novel object recognition, with minimal effect at 3 mg/kg [51], but no effect on contextual fear conditioning. In the current study, we did observe an effect of VU846 on neurophysiological features in WT mice, with decreased ESRP >20 Hz in the time window of 100–240 ms following the stimulation after 3 mg/kg treatment (Fig. 2B, top right panel, red dotted area), and decreased basal EEG beta band power after 1 mg/kg treatment. However, we did not observe the same dramatic changes in the AEP in WT mice as we did in RTT mice. We hypothesize that this difference reflects potentially altered sensitivity to an M_1 PAM in RTT mice due to decreased M1 receptor expression in this disease context. These results suggest a potentially important pathophysiological change in RTT mice and provide guidance for future mechanistic exploration of the underlying neurocircuitry.

Previous studies have observed that abnormalities in the cholinergic system in RTT and increasing cholinergic tone in RTT animal models improved phenotypic responses [41–45,69,70]. We predict that improvements in AEP features in RTT mice after VU846 treatment are due to potentiating cholinergic tone. Studies in people or animals (not with RTT) also have shown that altering cholinergic tone affects AEP [71,72]. For examples, treatment with rivastigmine, a cholinesterase inhibitor, enhances AEP features and this effect is blocked by an mAChR antagonists [71,73]. Additionally, a study on vagal nerve stimulation (VNS) demonstrated that increased cholinergic tone enhances AEP evoked in the primary auditory cortex (A1) [74], further supporting the relationship between cholinergic signaling and AEP responses. Interestingly, cortical recordings found that the VNS-induced strengthening of the AEP response was observed in the superficial, but not the deep, cortical A1 layer. This cortical layer-specific response was proposed by the authors to be due to differences in cortical laminar ACh innervation, with increased ACh nerve terminal density in superficial compared to deep cortical layers [75]. Further, VNS-induced modulation of EEG oscillatory activity was more robustly observed in stimulus-evoked conditions compared to resting state [76–78], consistent with our results showing that VU846 treatment did not alter the basal EEG power but increased auditory event-related power in RTT mice. Finally, VNS treatment decreased auditory stimulus-specific adaptation only with repeated stimuli [74]. All of these findings suggest that VNS treatment affects sensory gain control [74], and that the modulation of cholinergic tone might be related to basal cholinergic activity, providing insight to the observed inverted U-shaped VU846 dose-response on AEP observed here.

Event-related potentials (ERPs), such as AEPs, are thought to reflect the synchronized firing of similarly oriented cortical pyramidal neurons during information processing elicited by a variety of sensory, cognitive or motor events [79,80]. Changes in EPR could reflect variation of neural network activity, capability of neuronal crosstalk, or alterations in the local excitatory/inhibitory (E/I) balance [58,81–83]. Previous studies have shown that variation of local neurocircuit E/I balance alters AEPs evoked in RTT animal models [58]. In this study, we found that treatment with 3 mg/kg VU846 increased both AEP peak amplitudes and enhanced stimulus-driven neuronal synchronous activity, reflected by normalization of P2 latency, increased P2 rising and decay slope, decreased AEP waveform variation, and increased inter-trial phase coherence in RTT mice. Thus, it is possible that the improvement of VU846 on neural network synchronous activity occurs by its modulation of the local

neurocircuit cholinergic tone that then influences network E/I balance. Interestingly, VNS paired with sound stimulation in a rat model of RTT improved cortical A1 sound stimulus response and synchrony [84]. The effects of VNS on AEPs are thought to involve the modulation of sensory gain to enhance cortical output via a feedforward mechanism [74,85]. Thus, we hypothesize that a similar mechanism underlies the improvement of AEP by VU846 in RTT mice, in which VU846 treatment may shift the E/I balance within feedforward neurocircuitry in auditory processing pathways and result in the enhancement of auditory evoked responses [77,86–88].

Excitingly, Adcock et al. demonstrated that VNS treatment of a RTT rat model improved cortical response strength to sounds, supporting the concept that VNS treatment increased the auditory stimulus induced neural response and information [84]. Combined with previously observed effects of VNS on AEP, the connection of these effects to cholinergic signaling, and the role of modulating cholinergic tone in RTT to improve both AEP features and phenotypic abnormalities points to the therapeutic potential of cholinergic modulation in people with RTT. Importantly, positive modulation of M_1 cholinergic tone via VU846 did not increase epileptic discharges in RTT mice, which is important given the high incidence of seizures in people with RTT and previous work showing that PAMs with agonist activity at M_1 can induce seizures [51,89–91]. Future work is needed to further evaluate the effects of sub-acute or chronic dosing of VU846 on neurophysiological responses and phenotypic improvement to validate the utility of these neurophysiological features as biomarkers of treatment response. Furthermore, these findings provide both insight into and experimental approaches to characterize neural circuit level pathophysiological mechanisms in RTT related to cortical processing of sensory stimuli and the role of the cholinergic system in modulating cortical responses.

Authorship contribution statement

Conceptualization and Study Design: HWD, JLN, CMN.
Supervision and Project Administration: HWD, JLN, CMN.
Funding acquisition: HWD, JLN, CMN.
Methodology, Investigation, and Data Acquisition: HWD, KW, KB, MJM.
Formal Analysis: HWD.
Software: HWD.
Visualization and Illustration: HWD.
Writing-Original Draft: HWD and JLN.
Writing-Reviewing and Editing: HWD, JLN, CMN, KW, KB, MJM, CMN.

Submission declaration

The work described in this article has not been published previously or is under consideration for publication elsewhere. All authors have approved the submission of this article.

Declaration of competing interest

The authors declare the following financial interests/personal relationships which may be considered as potential competing interests: Jeffrey Neul reports financial support was provided by National Institute for Child Health and Development. Jeffrey Neul reports financial support was provided by International Rett Syndrome Foundation. Colleen Niswender reports financial support was provided by International Rett Syndrome Foundation. Colleen Niswender reports a relationship with ACADIA Pharmaceuticals Inc that includes: funding grants. Colleen Niswender reports a relationship with Neumora Therapeutics that includes: funding grants. Colleen Niswender received royalties from Acadia Pharmaceutical and Neumora Therapeutics for various classes of muscarinic receptor modulators. If there are other authors, they declare that they have no known competing financial interests or personal relationships that could have appeared to influence the work reported in this paper.

Acknowledgments

This work was supported by Vanderbilt Kennedy Cener Director's Strategic Priorities Pilot Grant (CMN and HWD), a grant from the International Rett Syndrome Foundation (#3906, JLN and CMN), the Eunice Kennedy Shriver National Institute of Child Health and Human Development (P50HD103537, JLN), and the Annette Schaffer Eskind Chair Fund (JLN). Rodent experiments were performed using the Murine Neurobehavior Core lab at the Vanderbilt University Medical Center. The content is solely the responsibility of the authors and does not necessarily represent the official views of the National Institutes of Health (NIH) or the Eunice Kennedy Shriver National Institute of Child Health and Human Development (NICHD). The funding sources had no role in the study design, interpretation, manuscript writing, or decision to submit the article for publication.

Appendix A. Supplementary data

Supplementary data to this article can be found online at https://doi.org/10.1016/j.neurot.2024.e00384.

References

[1] Neul JL, Kaufmann WE, Glaze DG, Christodoulou J, Clarke AJ, Bahi-Buisson N, et al. Rett syndrome: revised diagnostic criteria and nomenclature. Ann Neurol 2010;68(6):944–50.
[2] Amir RE, Van den Veyver IB, Wan M, Tran CQ, Francke U, Zoghbi HY. Rett syndrome is caused by mutations in X-linked MECP2, encoding methyl-CpG-binding protein 2. Nat Genet 1999;23(2):185–8.
[3] Cuddapah VA, Pillai RB, Shekar KV, Lane JB, Motil KJ, Skinner SA, et al. Methyl-CpG-binding protein 2 (MECP2) mutation type is associated with disease severity in Rett syndrome. J Med Genet 2014;51(3):152–8.
[4] Tarquinio DC, Hou W, Berg A, Kaufmann WE, Lane JB, Skinner SA, et al. Longitudinal course of epilepsy in Rett syndrome and related disorders. Brain 2017;140(2):306–18.
[5] Tarquinio DC, Hou W, Neul JL, Berkmen GK, Drummond J, Aronoff E, et al. The course of awake breathing disturbances across the lifespan in Rett syndrome. Brain Dev 2018;40(7):515–29.
[6] McCauley MD, Wang T, Mike E, Herrera J, Beavers DL, Huang TW, et al. Pathogenesis of lethal cardiac arrhythmias in mecp2 mutant mice: implication for therapy in rett syndrome. Sci Transl Med 2011;3(113):113ra125.
[7] Fu C, Armstrong D, Marsh E, Lieberman D, Motil K, Witt R, et al. Multisystem comorbidities in classic Rett syndrome: a scoping review. BMJ Paediatr Open 2020;4(1):e000731.
[8] Fu C, Armstrong D, Marsh E, Lieberman D, Motil K, Witt R, et al. Consensus guidelines on managing Rett syndrome across the lifespan. BMJ Paediatr Open 2020;4(1):e000717.
[9] Neul JL, Zoghbi HY. Rett syndrome: a prototypical neurodevelopmental disorder. Neuroscientist 2004;10(2):118–28.
[10] Zoghbi HY. MeCP2 dysfunction in humans and mice. J Child Neurol 2005;20(9):736–40.
[11] Collins BE, Neul JL. Rett syndrome and MECP2 Duplication syndrome: disorders of MeCP2 dosage. Neuropsychiatric Dis Treat 2022;18:2813–35.
[12] Guy J, Gan J, Selfridge J, Cobb S, Bird A. Reversal of neurological defects in a mouse model of rett syndrome. Science 2007;315:1143–7.
[13] Lang M, Wither RG, Colic S, Wu C, Monnier PP, Bardakjian BL, et al. Rescue of behavioral and EEG deficits in male and female Mecp2-deficient mice by delayed Mecp2 gene reactivation. Hum Mol Genet 2014;23(2):303–18.
[14] Kron M, Howell CJ, Adams IT, Ransbottom M, Christian D, Ogier M, et al. Brain activity mapping in Mecp2 mutant mice reveals functional deficits in forebrain circuits, including key nodes in the default mode network, that are reversed with ketamine treatment. J Neurosci 2012;32(40):13860–72.
[15] Patrizi A, Picard N, Simon AJ, Gunner G, Centofante E, Andrews NA, et al. Chronic administration of the N-Methyl-D-Aspartate receptor antagonist ketamine improves rett syndrome phenotype. Biol Psychiatr 2016;79(9):755–64.
[16] Gogliotti RG, Senter RK, Fisher NM, Adams J, Zamorano R, Walker AG, et al. mGlu7 potentiation rescues cognitive, social, and respiratory phenotypes in a mouse model of Rett syndrome. Sci Transl Med 2017;9(403).
[17] Gogliotti RG, Senter RK, Rook JM, Ghoshal A, Zamorano R, Malosh C, et al. mGlu5 positive allosteric modulation normalizes synaptic plasticity defects and motor phenotypes in a mouse model of Rett syndrome. Hum Mol Genet 2016;25(10):1990–2004.
[18] Banerjee A, Miller MT, Li K, Sur M, Kaufmann WE. Towards a better diagnosis and treatment of Rett syndrome: a model synaptic disorder. Brain 2019;142(2):239–48.

[19] Castro J, Garcia RI, Kwok S, Banerjee A, Petravicz J, Woodson J, et al. Functional recovery with recombinant human IGF1 treatment in a mouse model of Rett Syndrome. Proc Natl Acad Sci USA 2014;111(27):9941–6.
[20] Tropea D, Giacometti E, Wilson NR, Beard C, McCurry C, Fu DD, et al. Partial reversal of Rett Syndrome-like symptoms in MeCP2 mutant mice. Proc Natl Acad Sci USA 2009;106(6):2029–34.
[21] Pitcher MR, Ward CS, Arvide EM, Chapleau CA, Pozzo-Miller L, Hoeflich A, et al. Insulinotropic treatments exacerbate metabolic syndrome in mice lacking MeCP2 function. Hum Mol Genet 2013;22(13):2626–33.
[22] Tillotson R, Selfridge J, Koerner MV, Gadalla KKE, Guy J, De Sousa D, et al. Radically truncated MeCP2 rescues Rett syndrome-like neurological defects. Nature 2017;550(7676):398–401.
[23] Gadalla KKE, Vudhironarit T, Hector RD, Sinnett S, Bahey NG, Bailey MES, et al. development of a novel AAV gene therapy cassette with improved safety features and efficacy in a mouse model of rett syndrome. Mol Ther Methods Clin Dev 2017; 5:180–90.
[24] Sinnett SE, Gray SJ. Recent endeavors in MECP2 gene transfer for gene therapy of Rett syndrome. Discov Med 2017;24(132):153–9.
[25] Sinnett SE, Hector RD, Gadalla KKE, Heindel C, Chen D, Zaric V, et al. Improved MECP2 gene therapy extends the survival of MeCP2-null mice without apparent toxicity after intracisternal delivery. Mol Ther Methods Clin Dev 2017;5:106–15.
[26] Singh J, Goodman-Vincent E, Santosh P. Evidence synthesis of gene therapy and gene editing from different disorders-implications for individuals with rett syndrome: a systematic review. Int J Mol Sci 2023;24(10).
[27] Sripathy S, Leko V, Adrianse RL, Loe T, Foss EJ, Dalrymple E, et al. Screen for reactivation of MeCP2 on the inactive X chromosome identifies the BMP/TGF-beta superfamily as a regulator of XIST expression. Proc Natl Acad Sci USA 2017;114(7): 1619–24.
[28] Adrianse RL, Smith K, Gatbonton-Schwager T, Sripathy SP, Lao U, Foss EJ, et al. Perturbed maintenance of transcriptional repression on the inactive X-chromosome in the mouse brain after Xist deletion. Epigenet Chromatin 2018;11(1):50.
[29] Przanowski P, Wasko U, Zheng Z, Yu J, Sherman R, Zhu LJ, et al. Pharmacological reactivation of inactive X-linked Mecp2 in cerebral cortical neurons of living mice. Proc Natl Acad Sci USA 2018;115(31):7991–6.
[30] Carrette LLG, Wang CY, Wei C, Press W, Ma W, Kelleher 3rd RJ, et al. A mixed modality approach towards Xi reactivation for Rett syndrome and other X-linked disorders. Proc Natl Acad Sci USA 2018;115(4):E668–75.
[31] Merritt JK, Collins BE, Erickson KR, Dong H, Neul JL. Pharmacological read-through of R294X Mecp2 in a novel mouse model of Rett syndrome. Hum Mol Genet 2020;29(15):2461–70.
[32] Abdala AP, Lioy DT, Garg SK, Knopp SJ, Paton JF, Bissonnette JM. Effect of Sarizotan, a 5-HT1a and D2-like receptor agonist, on respiration in three mouse models of Rett syndrome. Am J Respir Cell Mol Biol 2014;50(6):1031–9.
[33] Gallo EF. Disentangling the diverse roles of dopamine D2 receptors in striatal function and behavior. Neurochem Int 2019;125:35–46.
[34] Tang X, Drotar J, Li K, Clairmont CD, Brumm AS, Sullins AJ, et al. Pharmacological enhancement of KCC2 gene expression exerts therapeutic effects on human Rett syndrome neurons and Mecp2 mutant mice. Sci Transl Med 2019;11(503).
[35] Neul JL, Percy AK, Benke TA, Berry-Kravis EM, Glaze DG, Marsh ED, et al. Trofinetide for the treatment of Rett syndrome: a randomized phase 3 study. Nat Med 2023;29(6):1468–75.
[36] Roche KJ, LeBlanc JJ, Levin AR, O'Leary HM, Baczewski LM, Nelson CA. Electroencephalographic spectral power as a marker of cortical function and disease severity in girls with Rett syndrome. J Neurodev Disord 2019;11(1):15.
[37] Saby JN, Benke TA, Peters SU, Standridge SM, Matsuzaki J, Cutri-French C, et al. Multisite study of evoked potentials in rett syndrome. Ann Neurol 2021;89(4): 790–802.
[38] Dong HW, Erickson K, Lee JR, Merritt J, Fu C, Neul JL. Detection of neurophysiological features in female R255X MeCP2 mutation mice. Neurobiol Dis 2020;145:105083.
[39] Goffin D, Allen M, Zhang L, Amorim M, Wang IT, Reyes AR, et al. Rett syndrome mutation MeCP2 T158A disrupts DNA binding, protein stability and ERP responses. Nat Neurosci 2012;15(2):274–83.
[40] Lamonica JM, Kwon DY, Goffin D, Fenik P, Johnson BS, Cui Y, et al. Elevating expression of MeCP2 T158M rescues DNA binding and Rett syndrome-like phenotypes. J Clin Invest 2017;127(5):1889–904.
[41] Wenk GL, Mobley SL. Choline acetyltransferase activity and vesamicol binding in Rett syndrome and in rats with nucleus basalis lesions. Neuroscience 1996;73(1): 79–84.
[42] Johnston MV, Hohmann C, Blue ME. Neurobiology of rett syndrome. Neuropediatrics 1995;26(2):119–22.
[43] Murasawa H, Kobayashi H, Imai J, Nagase T, Soumiya H, Fukumitsu H. Substantial acetylcholine reduction in multiple brain regions of Mecp2-deficient female rats and associated behavioral abnormalities. PLoS One 2021;16(10):e0258830.
[44] Gogliotti RG, Fisher NM, Stansley BJ, Jones CK, Lindsley CW, Conn PJ, et al. Total RNA sequencing of rett syndrome autopsy samples identifies the M4 muscarinic receptor as a novel therapeutic target. J Pharmacol Exp Therapeut 2018;365(2): 291–300.
[45] Smith M, Arthur B, Cikowski J, Holt C, Gonzalez S, Fisher NM, et al. Clinical and preclinical evidence for M(1) muscarinic acetylcholine receptor potentiation as a therapeutic approach for rett syndrome. Neurotherapeutics 2022;19(4):1340–52.
[46] Ballinger EC, Schaaf CP, Patel AJ, de Maio A, Tao H, Talmage DA, et al. Mecp2 deletion from cholinergic neurons selectively impairs recognition memory and disrupts cholinergic modulation of the perirhinal cortex. eNeuro 2019;6(6).
[47] Zhang Y, Zhu Y, Cao SX, Sun P, Yang JM, Xia YF, et al. MeCP2 in cholinergic interneurons of nucleus accumbens regulates fear learning. Elife 2020;9.
[48] Herrera JA, Ward CS, Wehrens XH, Neul JL. Methyl-CpG binding-protein 2 function in cholinergic neurons mediates cardiac arrhythmogenesis. Hum Mol Genet 2016; 25(22):4983–95.
[49] Zhang S, Johnson CM, Cui N, Xing H, Zhong W, Wu Y, et al. An optogenetic mouse model of rett syndrome targeting on catecholaminergic neurons. J Neurosci Res 2016;94(10):896–906.
[50] Nag N, Berger-Sweeney JE. Postnatal dietary choline supplementation alters behavior in a mouse model of Rett syndrome. Neurobiol Dis 2007;26(2):473–80.
[51] Rook JM, Bertron JL, Cho HP, Garcia-Barrantes PM, Moran SP, Maksymetz JT, et al. A novel M(1) PAM VU0486846 exerts efficacy in cognition models without displaying agonist activity or cholinergic toxicity. ACS Chem Neurosci 2018;9(9): 2274–85.
[52] Dwomoh L, Rossi M, Scarpa M, Khajehali E, Molloy C, Herzyk P, et al. M(1) muscarinic receptor activation reduces the molecular pathology and slows the progression of prion-mediated neurodegenerative disease. Sci Signal 2022;15(760): eabm3720.
[53] Voytek B, Kramer MA, Case J, Lepage KQ, Tempesta ZR, Knight RT, et al. Age-related changes in 1/f neural electrophysiological noise. J Neurosci 2015;35(38): 13257–65.
[54] Cohen MX. Analyzing neural time series data: theory and practice. The MIT Press; 2014.
[55] Maris E, Oostenveld R. Nonparametric statistical testing of EEG- and MEG-data. J Neurosci Methods 2007;164(1):177–90.
[56] Oostenveld R, Fries P, Maris E, Schoffelen JM. FieldTrip: open source software for advanced analysis of MEG, EEG, and invasive electrophysiological data. Comput Intell Neurosci 2011;2011:156869.
[57] Dong E, Agis-Balboa RC, Simonini MV, Grayson DR, Costa E, Guidotti A. Reelin and glutamic acid decarboxylase67 promoter remodeling in an epigenetic methionine-induced mouse model of schizophrenia. Proc Natl Acad Sci USA 2005;102(35): 12578–83.
[58] Goffin D, Brodkin ES, Blendy JA, Siegel SJ, Zhou Z. Cellular origins of auditory event-related potential deficits in Rett syndrome. Nat Neurosci 2014;17(6): 804–6.
[59] Wither RG, Colic S, Bardakjian BL, Snead 3rd OC, Zhang L, Eubanks JH. Electrographic and pharmacological characterization of a progressive epilepsy phenotype in female MeCP2-deficient mice. Epilepsy Res 2018;140:177–83.
[60] Saby JN, Peters SU, Roberts TPL, Nelson CA, Marsh ED. Evoked potentials and EEG analysis in rett syndrome and related developmental encephalopathies: towards a biomarker for translational research. Front Integr Neurosci 2020;14:30.
[61] Foxe JJ, Burke KM, Andrade GN, Djukic A, Frey HP, Molholm S. Automatic cortical representation of auditory pitch changes in Rett syndrome. J Neurodev Disord 2016;8(1):34.
[62] Stauder JE, Smeets EE, van Mil SG, Curfs LG. The development of visual- and auditory processing in Rett syndrome: an ERP study. Brain Dev 2006;28(8):487–94.
[63] LeBlanc JJ, DeGregorio G, Centofante E, Vogel-Farley VK, Barnes K, Kaufmann WE, et al. Visual evoked potentials detect cortical processing deficits in Rett syndrome. Ann Neurol 2015;78(5):775–86.
[64] Sysoeva OV, Molholm S, Djukic A, Frey HP, Foxe JJ. Atypical processing of tones and phonemes in Rett Syndrome as biomarkers of disease progression. Transl Psychiatry 2020;10(1):188.
[65] Bertron JL, Cho HP, Garcia-Barrantes PM, Panarese JD, Salovich JM, Nance KD, et al. The discovery of VU0486846: steep SAR from a series of M(1) PAMs based on a novel benzomorpholine core. Bioorg Med Chem Lett 2018; 28(12):2175–9.
[66] Dwomoh L, Tejeda GS, Tobin AB. Targeting the M1 muscarinic acetylcholine receptor in Alzheimer's disease. Neuronal Signal 2022;6(1):NS20210004.
[67] Abd-Elrahman KS, Sarasija S, Colson TL, Ferguson SSG. A positive allosteric modulator for the muscarinic receptor (M1 mAChR) improves pathology and cognitive deficits in female APPswe/PSEN1DeltaE9 mice. Br J Pharmacol 2022; 179(8):1769–83.
[68] Cikowski J, Holt C, Arthur B, Smith M, Gonzalez S, Lindsley CW, et al. Optimized administration of the M(4) PAM VU0467154 demonstrates broad efficacy, but limited effective concentrations in Mecp2(+/-) mice. ACS Chem Neurosci 2022; 13(13):1891–901.
[69] Wenk GL, Naidu S, Casanova MF, Kitt CA, Moser H. Altered neurochemical markers in Rett's syndrome. Neurology 1991;41(11):1753–6.
[70] Wenk GL, Hauss-Wegrzyniak B. Altered cholinergic function in the basal forebrain of girls with Rett syndrome. Neuropediatrics 1999;30(3):125–9.
[71] Klinkenberg I, Blokland A, Riedel WJ, Sambeth A. Cholinergic modulation of auditory processing, sensory gating and novelty detection in human participants. Psychopharmacology (Berl). 2013;225(4):903–21.
[72] Klinkenberg I, Sambeth A, Blokland A. Cholinergic gating of hippocampal auditory evoked potentials in freely moving rats. Eur Neuropsychopharmacol 2013;23(8): 988–97.
[73] Zhang J, Ma L, Li W, Yang P, Qin L. Cholinergic modulation of auditory steady-state response in the auditory cortex of the freely moving rat. Neuroscience 2016;324: 29–39.
[74] Takahashi H, Shiramatsu TI, Hitsuyu R, Ibayashi K, Kawai K. Vagus nerve stimulation (VNS)-induced layer-specific modulation of evoked responses in the sensory cortex of rats. Sci Rep 2020;10(1):8932.
[75] Chavez C, Zaborszky L. Basal forebrain cholinergic-auditory cortical network: primary versus nonprimary auditory cortical areas. Cerebr Cortex 2017;27(3): 2335–47.
[76] Sharon O, Fahoum F, Nir Y. Transcutaneous vagus nerve stimulation in humans induces pupil dilation and attenuates alpha oscillations. J Neurosci 2021;41(2): 320–30.

[77] Lewine JD, Paulson K, Bangera N, Simon BJ. Exploration of the impact of brief noninvasive vagal nerve stimulation on EEG and event-related potentials. Neuromodulation 2019;22(5):564–72.
[78] Schuerman WL, Nourski KV, Rhone AE, Howard MA, Chang EF, Leonard MK. Human intracranial recordings reveal distinct cortical activity patterns during invasive and non-invasive vagus nerve stimulation. Sci Rep 2021;11(1):22780.
[79] Blackwood DH, Muir WJ. Cognitive brain potentials and their application. Br J Psychiatr Suppl 1990;9:96–101.
[80] Peterson NN, Schroeder CE, Arezzo JC. Neural generators of early cortical somatosensory evoked potentials in the awake monkey. Electroencephalogr Clin Neurophysiol 1995;96(3):248–60.
[81] Tan AY, Wehr M. Balanced tone-evoked synaptic excitation and inhibition in mouse auditory cortex. Neuroscience 2009;163(4):1302–15.
[82] Dorrn AL, Yuan K, Barker AJ, Schreiner CE, Froemke RC. Developmental sensory experience balances cortical excitation and inhibition. Nature 2010;465(7300):932–6.
[83] Tada M, Kirihara K, Koshiyama D, Fujioka M, Usui K, Uka T, et al. Gamma-band auditory steady-state response as a neurophysiological marker for excitation and inhibition balance: a review for understanding schizophrenia and other neuropsychiatric disorders. Clin EEG Neurosci 2020;51(4):234–43.
[84] Adcock KS, Chandler C, Buell EP, Solorzano BR, Loerwald KW, Borland MS, et al. Vagus nerve stimulation paired with tones restores auditory processing in a rat model of Rett syndrome. Brain Stimul 2020;13(6):1494–503.
[85] Kumagai S, Shiramatsu TI, Matsumura A, Ishishita Y, Ibayashi K, Onuki Y, et al. Frequency-specific modulation of oscillatory activity in the rat auditory cortex by vagus nerve stimulation. Brain Stimul 2023;16(5):1476–85.
[86] Markov NT, Vezoli J, Chameau P, Falchier A, Quilodran R, Huissoud C, et al. Anatomy of hierarchy: feedforward and feedback pathways in macaque visual cortex. J Comp Neurol 2014;522(1):225–59.
[87] Rodenkirch C, Wang Q. Rapid and transient enhancement of thalamic information transmission induced by vagus nerve stimulation. J Neural Eng 2020;17(2):026027.
[88] Michalareas G, Vezoli J, van Pelt S, Schoffelen JM, Kennedy H, Fries P. Alpha-beta and gamma rhythms subserve feedback and feedforward influences among human visual cortical areas. Neuron 2016;89(2):384–97.
[89] Engers JL, Childress ES, Long MF, Capstick RA, Luscombe VB, Cho HP, et al. VU6007477, a novel M(1) PAM based on a pyrrolo[52]pyridine carboxamide core devoid of cholinergic adverse events. ACS Med Chem Lett 2018;9(9):917–22.
[90] Moran SP, Cho HP, Maksymetz J, Remke DH, Hanson RM, Niswender CM, et al. PF-06827443 displays robust allosteric agonist and positive allosteric modulator activity in high receptor reserve and native systems. ACS Chem Neurosci 2018;9(9):2218–24.
[91] Davoren JE, Garnsey M, Pettersen B, Brodney MA, Edgerton JR, Fortin JP, et al. Design and synthesis of gamma- and delta-lactam M(1) positive allosteric modulators (PAMs): convulsion and cholinergic toxicity of an M(1)-selective PAM with weak agonist activity. J Med Chem 2017;60(15):6649–63.